Electronic Supplementary Material (ESI) for Journal of Materials Chemistry A.

Supporting Information for

Rational Encapsulation of Atomically Precise Nanoclusters into Metal-Organic Frameworks by Electrostatic Attraction for CO_2 Conversion

Lili Sun,† Yapei Yun,† Hongting Sheng,* Yuanxin Du, Yimin Ding, Pei Wu, Peng Li, Manzhou Zhu*

Department of Chemistry and Center for Atomic Engineering of Advanced Materials, AnHui Province Key Laboratory of Chemistry for Inorganic/Organic Hybrid Functionalized Materials, Anhui University, Hefei, Anhui 230601, China

E-mail: sht_anda@126.com; zmz@ahu.edu.cn

† L. Sun and Y. Yun contributed equally.

Materials

All reagents were analytical grade and were used without further processed.

Experimental Section

1. Preparation of ZIF-8 dodecahedron.

2-MeIM (25 mmol) and Zn $(NO_3)_2 \cdot 6H_2O$ (25 mmol) were dissolved in 20 mL methanol, respectively. After that, 2-MeIM solution and Zn-salt solution were mixed together. The mix solution aged for 24 hours at room temperature. The product was collected by centrifugation (10,000 rpm) for 5 mins and washed with MeOH five times. At last, ZIF-8 was dried at 60 °C for 5 hours.

2. Preparation of ZIF-67 dodecahedron.

Typically, $Co(NO_3)_2$ (0.249 g) and 2-MeIM (0.328 g) was dispersed in 25 ml MeOH, respectively.Then the $Co(NO_3)_2$ solution was slowly poured into the 2-MeIM solution with obvious purple changes under vigorous stirring for 5 mins to form homogeneous solution at room temperature. After that, the mix solution aged for 24 hours. The precipitation was collected by centrifugation (10,000 rpm) for 5 mins and washed with MeOH for ten times, the ZIF-67 was dried at 60 °C for 5 hours.

3. Preparation of MHCF nanocubes.

A simple chemical method to synthesis the MHCF nanocubes that obtain from the previous report. First, $MnSO_4.H_2O$ (0.045 g) was dispersed in the mixed solvent system with 10 mL H_2O and 5 mL C_2H_5OH; Next, 10 mL H_2O of $K_3Fe(CN)_6$ (0.066 g) was pure into above solution and stirred for 90 mins at room temperature. After that, the black-gray product was collected by centrifugation (10,000 rpm) for 5 mins and washed ten times with ethanol and dried at 60°C for 5 hours.

4. Synthesis of $[Ag_{44}(SR)_{30}^{4-}][(PPh_4)_4^{4+}]$nanoclusters.

20 mg $AgNO_3$ were dissolved in 2 mL methanol and poured into 50mL reaction bulb with 10 mL dichloromethane. The mixture solution was kept 0°C with an ice bath, and then, 10 mL 3,4-difluorobenzenethiol and 12 mg tetraphenylphosphonium bromide were added, respectively. Stirring for 20 minutes, 50 μL triethylamine and 45mg $NaBH_4$ with 1mL deionized water were added quickly at a vigorous stirring for 12 hours at 0^o C. After the reaction stops, remove the water phase and the resulting

solution in the organic phase was desiccated in vacuum on a rotary evaporator and washed several times with water. The $(PPh_4)_4[Ag_{44}(SC_6H_3F_2)_{30}]$ nanoclusters were obtained.

5. Synthesis of $[Au_{12}Ag_{32}(SR)_{30}]^{4-}$ $[(PPh_4)_4]^{4+}$ nanoclusters.

10 mg of chloro(triphenylphosphine)gold(I) ($AuPPh_3Cl$) and 10 mg $AgNO_3$ were used instead of 20 mg $AgNO_3$ in the synthesis of $Ag_{44}(SR)_{30}$ nanoclusters. All the other conditions were remained unchanged. The $(PPh_4)_4[Au_{12}Ag_{32}(SC_6H_3F_2)_{30}]$ nanoclusters were obtained.

6. Synthesis of $[Ag_{28}Cu_{12}(SR)_{30}^{4-}][(C_{16}H_{36}N_4)^{4+}]$ nanoclusters.

10 mg of $AgNO_3$ was dissolved in 2 mL methanol, followed by the addition of 8 mg CuBr in 10 mL of dichloromethane. The mixture was cooled to 0 °C in an ice bath, 10 μL of 2,4-dichlorobenzenethiol and 6 mg of tetrabutylammonium bromide were added. After 20 mins stirring, 1 mL of an aqueous solution of $NaBH_4$ (40 mg/mL) and 50 μL of triethylamine were added quickly to the reaction mixture under vigorous stirring. The reaction mixture was aged for 12 h at 0 °C. The aqueous phase was then removed. The organic phase was washed several times with water and evaporated for further analysis. The $(C_{16}H_{36}N_4)$ $[Ag_{12}Cu_{28}(SC_6H_3Cl_2)_{30}]$ nanoclusters were obtained.

7. Synthesis of $[Ag_{46}Au_{24}(SR)_{32}]^{2+}$ $[(BPh_4)_2]^{2-}$ nanoclusters.

In summary, $AgNO_3$ and $HAuCl_4 \cdot 3H_2O$ were dissolved in methanol to give a yellow turbid liquid. Tertiary butyl was added into the solution to obtain the mixture of AuI-SR and AgI-SR complex. Then, NaOH (1 M) was used to adjust the pH value. After that, $NaBH_4$ was used to reduce this mixture complex. The $Ag_{46}Au_{24}(SR)_{32}^{2+}$ nanoclusters were precipitated out from the solution, washed by hexane, extracted by toluene, and redissolved in CH_2Cl_2 solution. The addition of $NaBPh_4$ (dissolved in methanol) formed $[Ag_{46}Au_{24}(SR)_{32}]$ $(BPh_4)_2$ nanoclusters.

8. Synthesis of APNCs@ZIF-8.

The synthesis of APNCs@ZIF-8 is easily to achieve. $Zn(NO_3)_2 \cdot 6H_2O$ (0.558 g) and APNCs (6mg) were dissolved in 10 mL methanol. The APNCs quickly assembled with positively charged Zn^{2+} by electrostatic attraction. Subsequently, 20 mL methanol solution of 2-MeIM (0.595 g) was slowly pureed into the above solution and

mixed together. After being aged for 24 h at room temperature, the solution was then centrifuged at 10,000 rpm for at least 5 min, and the precipitate was washed with MeOH five times, and then dried in an oven at 60 °C.

9. Synthesis of APNCs@ZIF-67.

$Co(NO_3)_2$ (0.249 g) and APNCs (6 mg) was dissolved in 12.5 ml methanol. The APNCs quickly assembled with positively charged Co^{2+} by electrostatic attraction. Subsequently, 20 mL methanol solution of 2-MeIM (0.328 g) was slowly pureed into the above solution and mixed together. After being aged for 24 hours at room temperature, the solution was then centrifuged at 10,000 rpm for at least 5 min, and the precipitate was washed with MeOH five times, and then dried in an oven at 60 °C.

10. Synthesis of APNCs@MHCF.

First, $MnSO_4 \cdot H_2O$ (0.045 g) was dispersed in the mixed solvent system with 10 mL H_2O and 5 mL ethanol; 5 mL ethanol solution of APNCs (6mg) was mix together with the above $MnSO_4$ solution. The APNCs quickly assembled with positively charged Mn^{2+} by electrostatic attraction. Next, 10 mL H_2O of $K_3Fe(CN)_6$ (0.066 g) was slowly poured into the mixed solution and stirred for 90 mins at room temperature. After that, the solution was centrifuged at 10,000 rpm for at least 5 min, and washed ten times with ethanol and dried at 60°C for 5 hours.

11. The catalytic activity of APNCs@MOFs for the carboxylation of phenylacetlene.

APNCs@MOFs (60 mg $Au_{12}Ag_{32}(SR)_{30}$@ZIF-8, (0.94 wt. % loading of $Au_{12}Ag_{32}(SR)_{30}^{4-}$; 5.5×10^{-5} mol) K_2CO_3 (0.24 mmol) were added to DMSO (1 mL) in the reaction tube. CO_2 (balloon, 1 atm) and phenylacetylene (1 mmol) were added to the reaction mixture under stirring at 50°C for 24 h. After the reaction, centrifugal separation the catalyst, and K_2CO_3 (138mg, 5 mL of water) was introduced into the reaction mixture via stirred for 30 min. Then, the mixture solution was extracted by 10ml dichloromethane with three times, and remove dichloromethane. After that, the aqueous phase was acidified with concentrated hydrochloric acid to pH=1, and the aqueous layer was extracted with dichloromethane three times again. Finally,

anhydrous Na_2SO_4 was added into the combined organic layers to eliminate a small amount of water, filtered and the resulting solution was desiccated in vacuum on a rotary evaporator, Obtain the weighing yield.

12. Materials characterization

UV−vis spectra were recorded on a Techcomp UV1000 spectrophotometer. The sample had been kept at 100°C for 1h before analysis. Scanning electron microscope was obtained on a */S-4800 microscope with an accelerating voltage of 0.1-30 kV. Transmission electron microscopy (TEM) was conducted on a JEM-2100 microscope with an accelerating voltage of 200 kV. FT-IR spectra were recorded with Bruker Tensor 27 instrument. X-ray diffraction (XRD) patterns were obtained on SmartLab 9KW with Cu Kα radiation. Nanoclusters loaded into the ZIF-8 catalyst were determined by Inductively Coupled Plasma Mass Spectrometry (ICP-MS). X-ray photoelectron spectroscopy (XPS) measurements were on ESCALAB 250Xi.

Figures and Tables

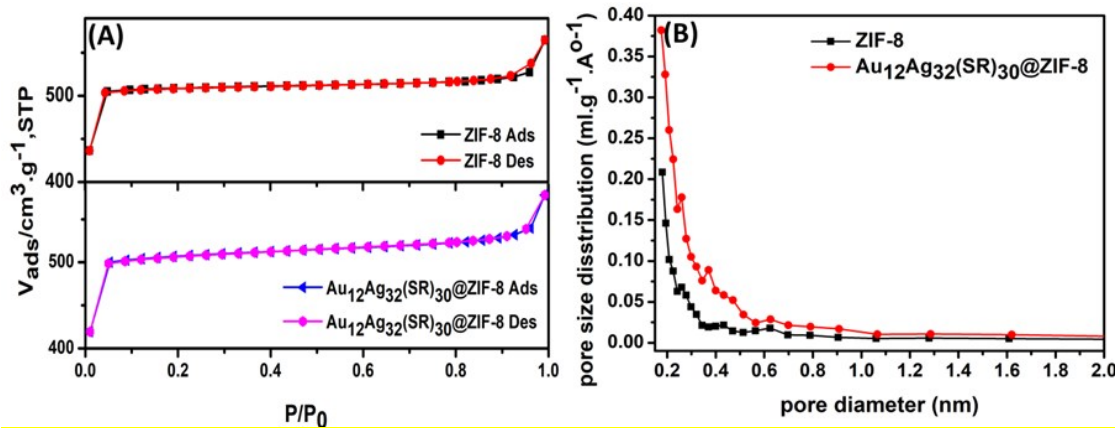

Fig. S1. A) N_2 absorption–desorption isothermal of $Au_{12}Ag_{32}(SR)_{30}$@ZIF-8 and ZIF-8. B) Pore size distribution of $Au_{12}Ag_{32}(SR)_{30}$@ZIF-8 and ZIF-8.

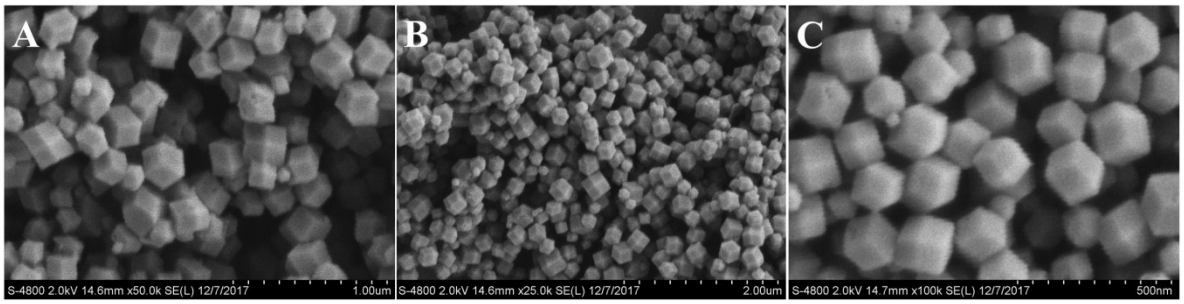

Fig S2. SEM images of the APNCs@ZIF-8 composites. (A) $Au_{12}Ag_{32}(SR)_{30}$@ZIF-8 composite, **(B)** the $Ag_{44}(SR)_{30}$@ZIF-8 composite, **(C)** the $Ag_{12}Cu_{28}(SR)_{30}$@ZIF-8 composite.

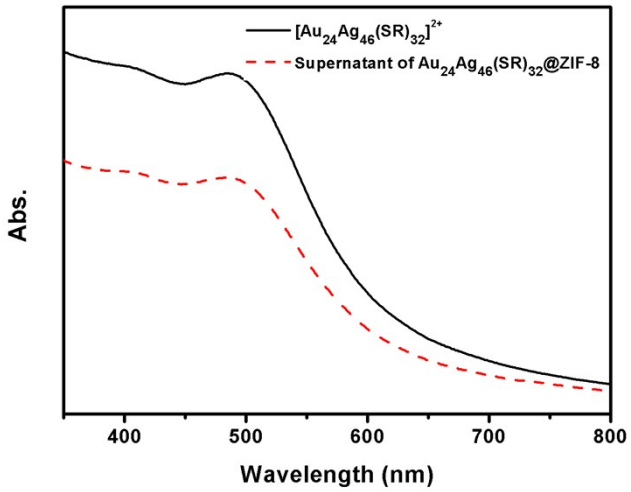

Fig. S3 The UV-vis spectrum of $[Au_{46}Ag_{24}(SR)_{32}]^{2+}$ nanoclusters and supernatant of $Au_{46}Ag_{24}(SR)_{32}$@ZIF-8.

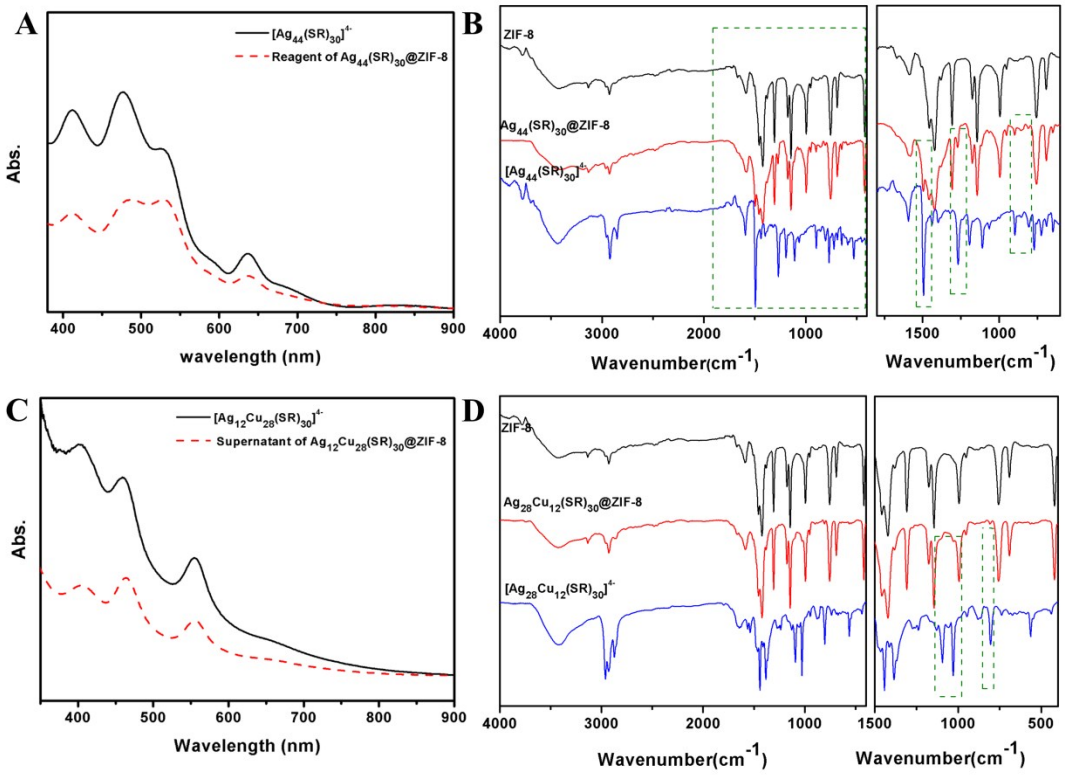

Fig. S4 The UV-vis spectrum of APNCs and supernatant of APNCs@ZIF-8 (the left). The FT-IR spectrum of ZIF-8, APNCs@ZIF-8 and APNCs (the right). The UV-vis spectrum of **(A)** $[Ag_{44}(SR)_{30}]^{4-}$ nanoclusters and reagent of $Ag_{44}(SR)_{30}$@ZIF-8, **(C)** $[Ag_{12}Cu_{28}(SR)_{30}]^{4-}$ nanoclusters and reagent of $Ag_{12}Cu_{28}(SR)_{30}$@ZIF-8, **(E)** $[Au_{25}(SR)_{18}]^{-}$ nanoclusters and reagent of $Au_{25}(SR)_{18}$@ZIF-8. The FT-IR spectrum of **(B)** ZIF-8, $Ag_{44}(SR)_{30}$@ZIF-8 and $[Ag_{44}(SR)_{30}]^{4-}$ nanoclusters; **(D)** ZIF-8, $Ag_{12}Cu_{28}(SR)_{30}$@ZIF-8 and $[Ag_{12}Cu_{28}(SR)_{30}]^{4-}$ nanoclusters; **(F)** ZIF-8, $Au_{25}(SR)_{18}$@ZIF-8 and$[Au_{25}(SR)_{18}]^{-}$ nanoclusters.

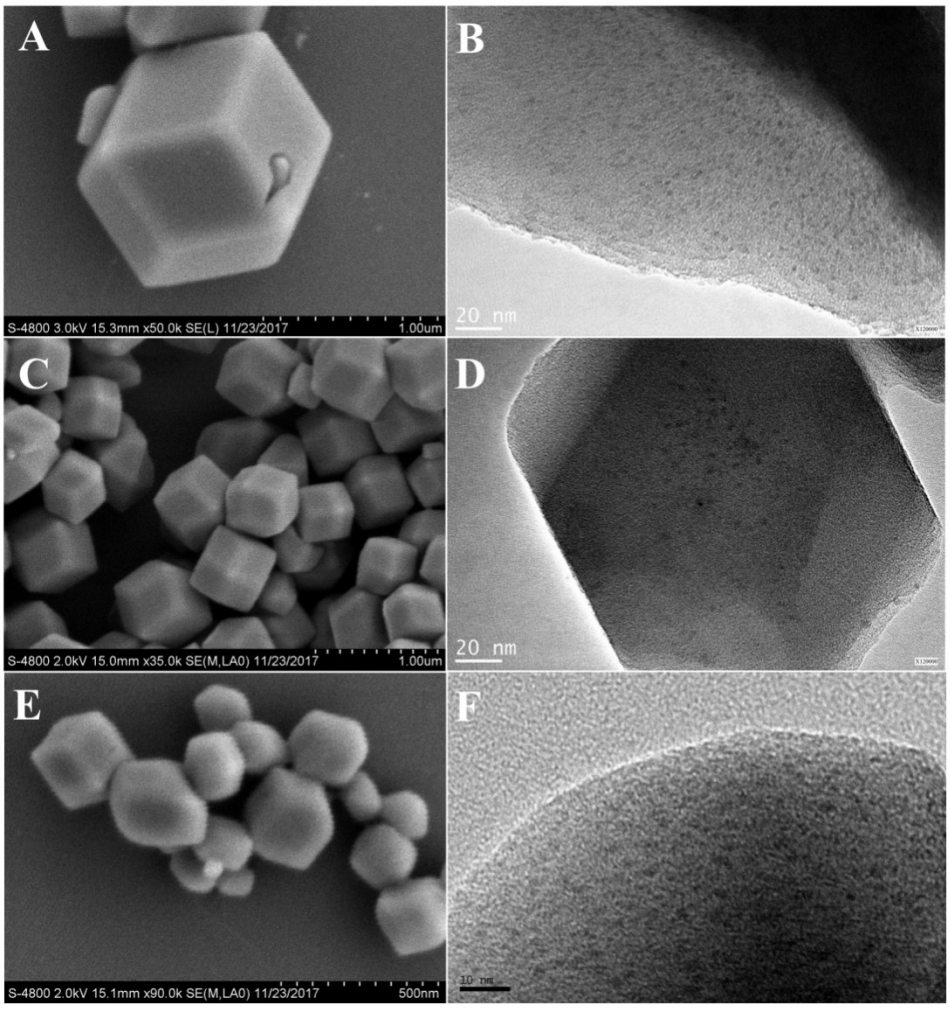

Fig. S5 The SEM and TEM images of APNCs@ZIF-67 composites. The SEM images of **(A)** $Au_{12}Ag_{32}(SR)_{30}$@ZIF-67, **(C)** $Ag_{44}(SR)_{30}$@ZIF-67 and **(E)** $Ag_{12}Cu_{28}(SR)_{30}$@ZIF-67. The TEM images of **(B)** $Au_{12}Ag_{32}(SR)_{30}$@ZIF-67, **(D)** $Ag_{44}(SR)_{30}$@ZIF-67 and **(F)** $Ag_{12}Cu_{28}(SR)_{30}$ @ZIF-67.

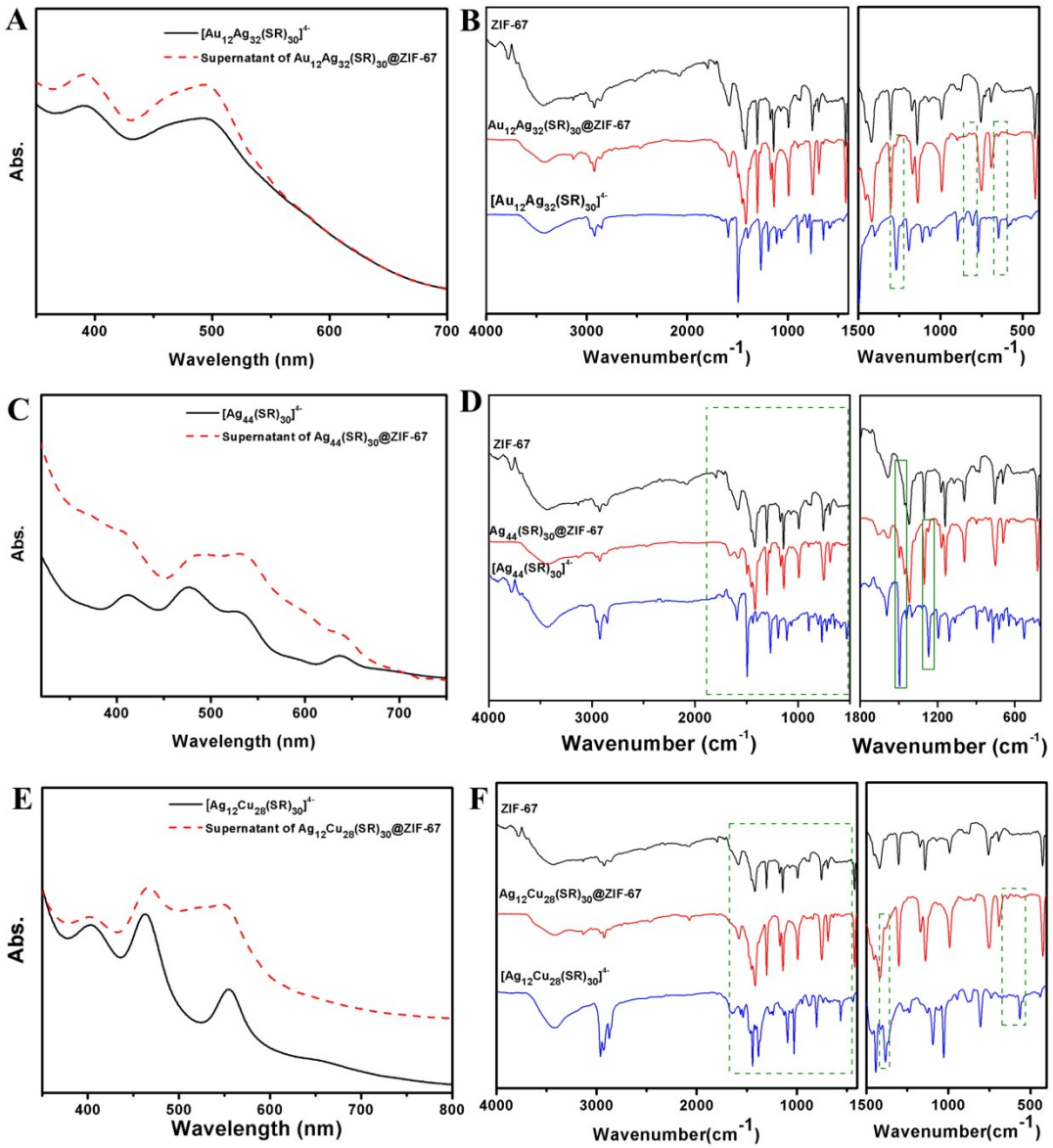

Fig. S6 The UV-vis spectrums of APNCs and Supernatant of APNCs@ZIF-67 (the left). The FT-IR spectrums of ZIF-67, APNCs@ZIF-67 and APNCs (the right). The UV-vis spectrum of **(A)** $[Au_{12}Ag_{32}(SR)_{30}]^{4-}$ nanoclusters and reagent of $Au_{12}Ag_{32}(SR)_{30}$@ZIF-67, **(C)** $[Ag_{44}(SR)_{30}]^{4-}$ nanoclusters and reagent of $Ag_{44}(SR)_{30}$@ZIF-67, **(E)** $[Ag_{12}Cu_{28}(SR)_{30}]^{4-}$ nanoclusters and reagent of $Ag_{12}Cu_{28}(SR)_{30}$@ZIF-67; The FT-IR spectrum of ZIF-67, **(B)** $Au_{12}Ag_{32}(SR)_{30}$@ZIF-67 and $[Au_{12}Ag_{32}(SR)_{30}]^{4-}$ nanoclusters; **(D)** ZIF-67, $Ag_{44}(SR)_{30}$@ZIF-67 and $[Ag_{44}(SR)_{30}]^{4-}$ nanoclusters; **(F)** ZIF-67, $Ag_{12}Cu_{28}(SR)_{30}$@ZIF-67 and[$Ag_{12}Cu_{28}(SR)_{30}$]$^{4-}$ nanoclusters;

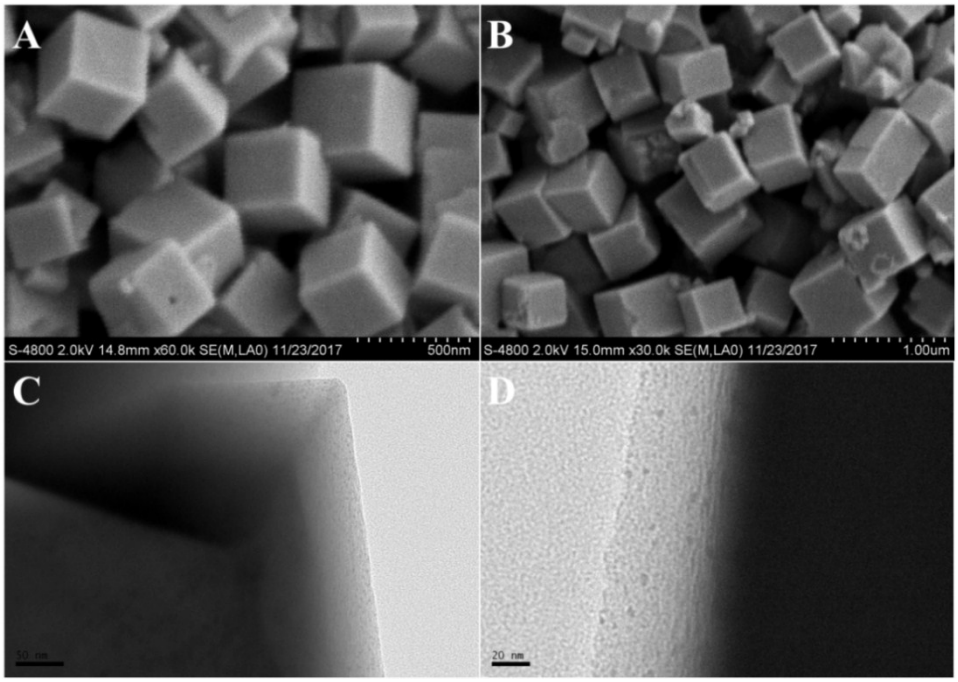

Fig. S7 The SEM and TEM images of APNCs@MHCF composites. The SEM images of **(A)** $Au_{12}Ag_{32}(SR)_{30}$@MHCF and **(B)** $Ag_{12}Cu_{28}(SR)_{30}$@MHCF. The TEM images of **(C)** $Au_{12}Ag_{32}(SR)_{30}$@MHCF and **(D)** $Ag_{12}Cu_{28}(SR)_{30}$@MHCF.

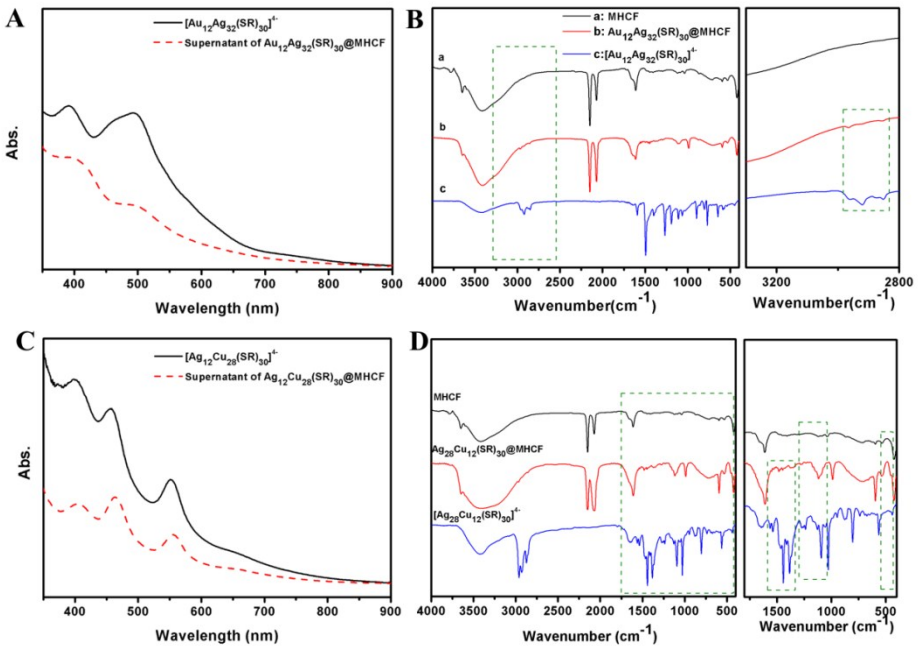

Fig. S8 The UV-vis spectrums of APNCs and Supernatant of APNCs@MHCF (the left). The FT-IR spectrums of MHCF, APNCs@MHCF and APNCs (the right). The UV-vis spectrum of **(A)** $[Au_{12}Ag_{32}(SR)_{30}]^{4-}$ nanoclusters and reagent of $Au_{12}Ag_{32}(SR)_{30}$@MHCF , **(C)** $[Ag_{12}Cu_{28}(SR)_{30}]^{4-}$ nanoclusters and reagent of $Ag_{12}Cu_{28}(SR)_{30}$@MHCF; The FT-IR spectrum of **(B)** MHCF, $Au_{12}Ag_{32}(SR)_{30}$@MHCF and $[Au_{12}Ag_{32}(SR)_{30}]^{4-}$ nanoclusters; **(D)** MHCF, $Ag_{12}Cu_{28}(SR)_{30}$@MHCF and $Ag_{12}Cu_{28}(SR)_{30}{}^{4-}$ nanoclusters.

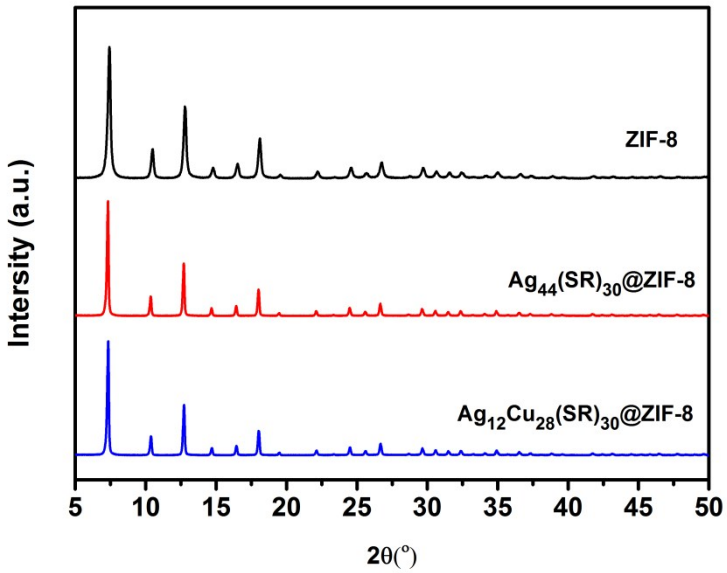

Fig. S9 the XRD patterns of ZIF-8, $Ag_{44}(SR)_{30}$@ZIF-8, $Ag_{12}Cu_{28}(SR)_{30}$@ZIF-8 .

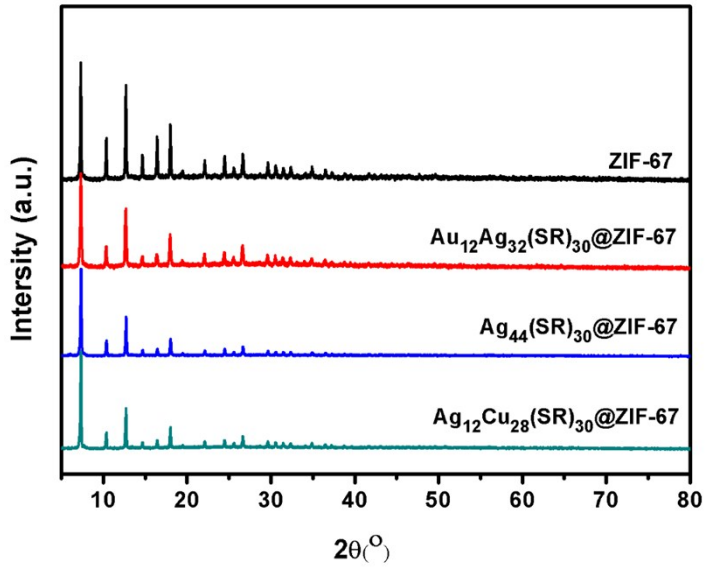

Fig. S10 the XRD patterns of ZIF-67, $Au_{12}Ag_{32}(SR)_{30}$@ZIF-67, $Ag_{44}(SR)_{30}$@ZIF-67, and $Ag_{12}Cu_{28}(SR)_{30}$@ZIF-67.

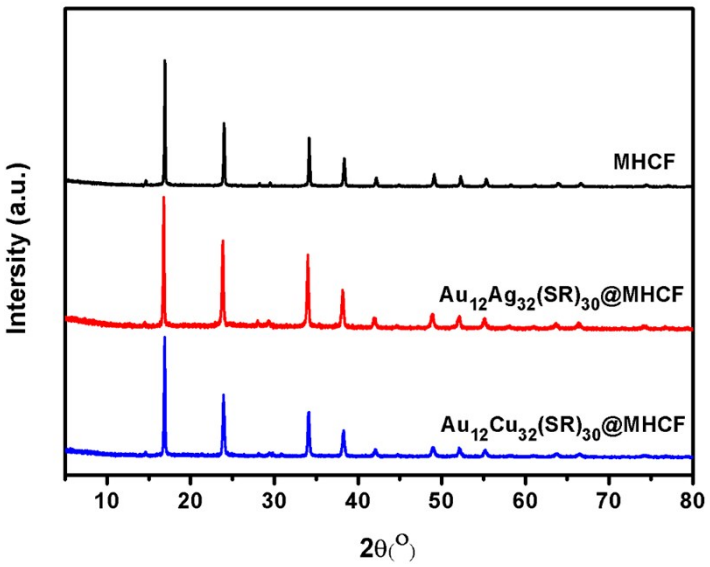

Fig. S11. the XRD patterns of MHCF, $Au_{12}Ag_{32}(SR)_{30}$@MHCF, and $Ag_{12}Cu_{28}(SR)_{30}$@MHCF.

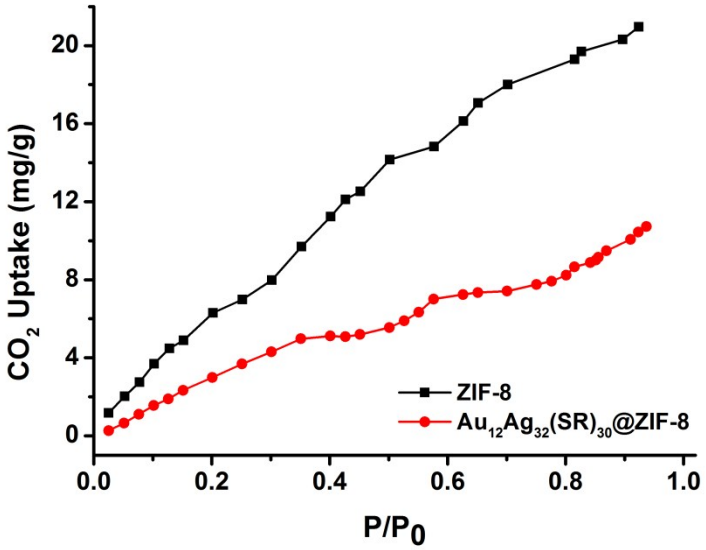

Fig. S12. the CO_2 adsorption−desorption isotherms of ZIF-8 and $Au_{12}Ag_{32}(SR)_{30}$@ZIF-8.

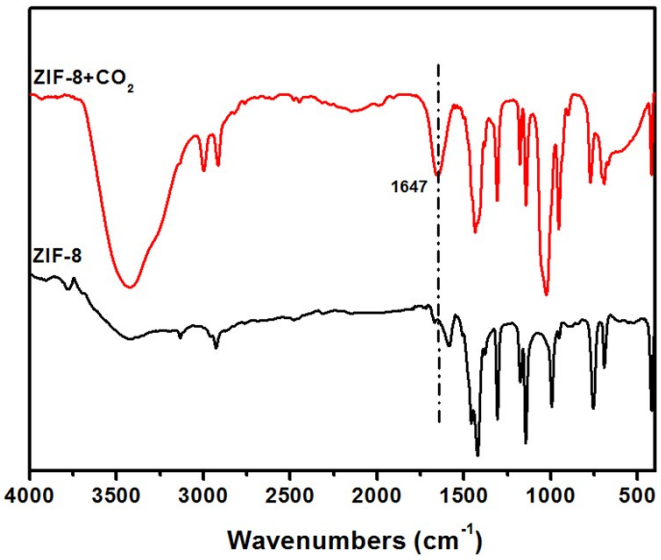

Fig. S13. The FT-IR spetrums of ZIF-8 and ZIF-8+CO_2.

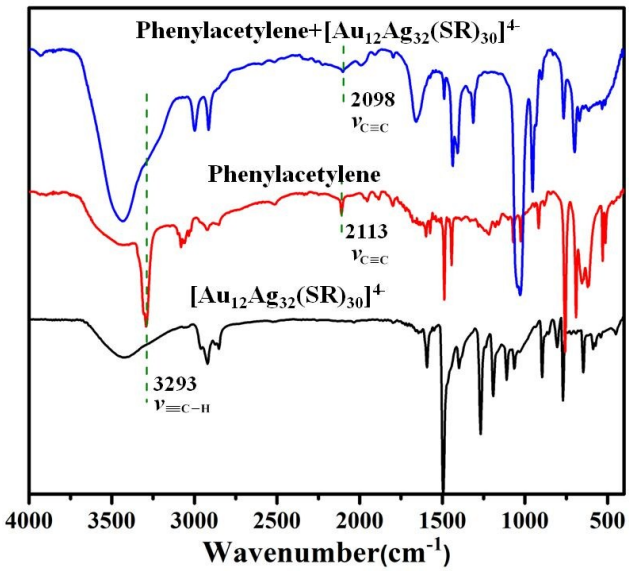

Fig. S14 The FT-IR spectra of phenylacetylene + $[Au_{12}Ag_{32}(SR)_{30}]^{4-}$ (blue curve), phenylacetylene (red curve) and $[Au_{12}Ag_{32}(SR)_{30}]^{4-}$ (black curve).

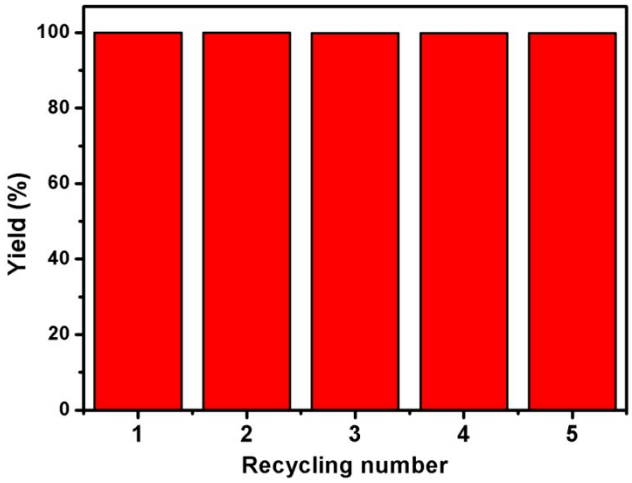

Fig. S15. The recycled of $Au_{12}Ag_{32}(SR)_{30}$@ZIF-8 catalyst for benzene acetylene carboxylation reaction.

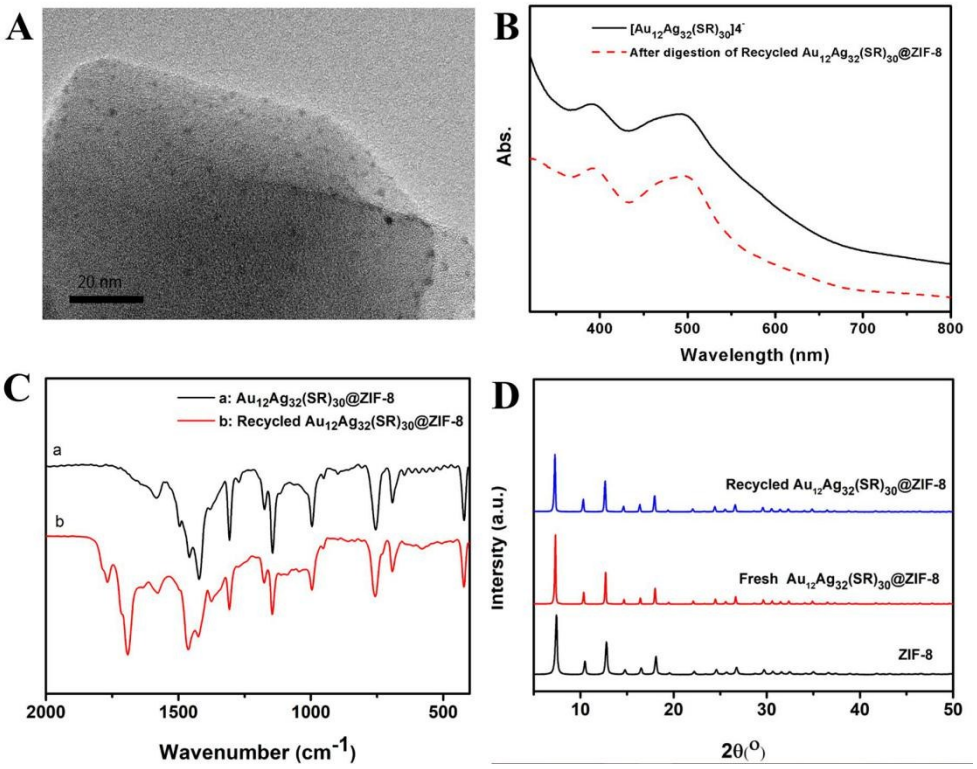

Fig. S16 The characterization of recycled $Au_{12}Ag_{32}(SR)_{30}$@ZIF-8. (A) TEM images of recycled; **(B)** the UV-vis spectrums of $[Au_{12}Ag_{32}(SR)_{30}]^{4-}$ nanoclusters and digestion of recycled $Au_{12}Ag_{32}(SR)_{30}$@ZIF-8; **(C)** the FT-IR spectrums of ZIF-8, recycled$Au_{12}Ag_{32}(SR)_{30}$@ZIF-8 and $[Au_{12}Ag_{32}(SR)_{30}]^{4-}$ nanoclusters; **(D)** the XRD patterns of ZIF-8 and recycled$Au_{12}Ag_{32}(SR)_{30}$@ZIF-8.

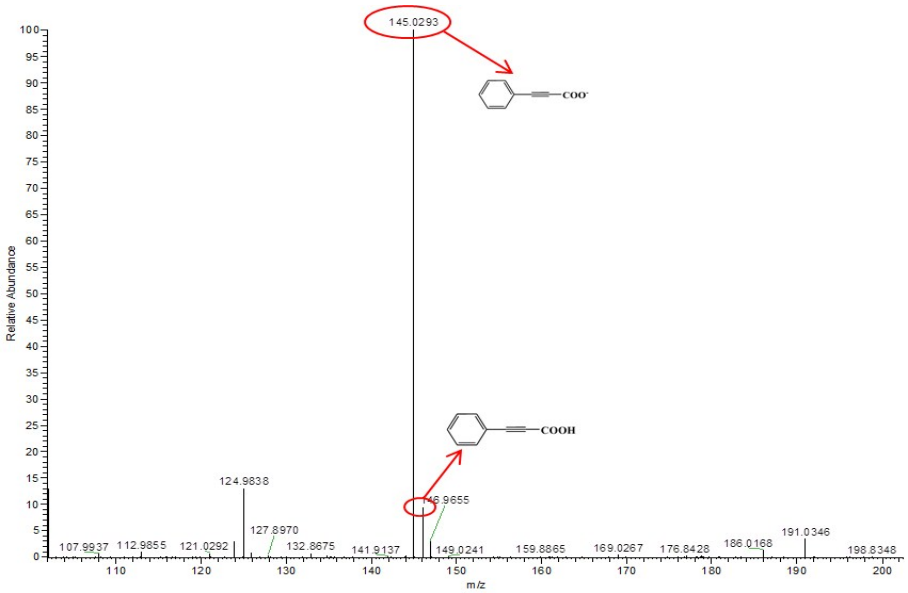

Fig. S17 ESI-MS of Phenylpropiolic acid. m/z=146.0

Table S1. Synthesis of 3-phenylpropiolic acid from CO_2 and 1-ethynylbenzene with catalysts.[a]

Entry	Catalyst	T (° C)	T (h)	Yields (%)	TON[b]	Refernce
1	Ag@MIL-101[c]	50	15	97	36	Ref.1
2	Ag@P-NHC[c]	25	20	98	327	Ref.2
3	Ag@Shiff-SiO_2	60	24	98	705	Ref.3
4	$Pd_{0.2}$-$Cu_{0.8}$/MIL-101[d]	25	24	96	691	Ref.4
5	Ag/KAPs-P	60	10	92	9936	Ref.5
6	Ag/F-Al_2O_3[d]	50	18	62	12	Ref.6
7	L_3/Ag[e]	35	24	98	392	Ref.7
8	{LNd[$N(SiMe_3)_2$].THF}$_2$[c]	60	24	72	23	Ref.8
9	$Au_{12}Ag_{32}(SR)_{30}$@ZIF-8[f]	50	24	>99.9	18164	This work

[a] **Reaction conditions:** 1-ethynylbenzene (1.0 mmol), Cs_2CO_3 (1.5 mmol), solvent (DMSO, 5 mL), CO_2 (1.0 atm). [b] TON = (moles of product)/(moles of metal in the catalyst). [c] Solvent (DMF, 5mL). [d] Solvent (DMSO, 5 mL), CO_2 (60atm). [e] 1-ethynylbenzene (10 mmol), Cs_2CO_3 (1.5 equiv.), Solvent (DMF, 40 mL).[f] K_2CO_3 (0.24 mmol), solvent (DMSO, 1mL).

Reference

1. X. H. Liu, J. G. Ma, Z. Niu, G. M. Yang, P. Cheng, An Efficient Nanoscale Heterogeneous Catalyst for the Capture and Conversion of Carbon Dioxide at Ambient Pressure. *Angew. Chem. Int. Ed.* **54**, 988-991 (2015)
2. D. Yu, M. X. Tan, Y. Zhang, Carboxylation of Terminal Alkynes with Carbon Dioxide Catalyzed by Poly(N-Heterocyclic Carbene)-Supported Silver Nanoparticles. *Adv. Synth. Catal.* **354**, 969-974 (2012)
3. Z. Wu, L. Sun, Q. Liu, X. Yang, X. Ye, Y. Hu, Y. Huang, A Schiff base-modified silver

catalyst for efficient fixation of CO_2 as carboxylic acid at ambient pressure. *Green Chem.* **19**, 2080-2085 (2017)

4. M. Trivedi, Bhaskaran, A. Kumar, G. Singh, A. Kumar, N. P. Rath, Metal–organic framework MIL-101 supported bimetallic Pd–Cu nanocrystals as efficient catalysts for chromium reduction and conversion of carbon dioxide at room temperature. *New J. Chem.* **40**, 3109-3118 (2016).
5. Z. Wu, Q. Liu, X. Yang, X. Ye, H. Duan, J. Zhang, B. Zhao, Y. Huang, Knitting Aryl Network Polymers-Incorporated Ag Nanoparticles: A Mild and Efficient Catalyst for the Fixation of CO_2 as Carboxylic Acid. *ACS Sustainable Chem. Eng.* **5,** 9634-9639 (2017).
6. E. D. Finashina, L. M. Kustov, O. P. Tkachenko, V. G. Krasovskiy, E. I. Formenova, I. P. Beletskaya, Carboxylation of phenylacetylene by carbon dioxide on heterogeneous Ag-containing catalysts. *Russ. Chem. B* **63,** 2652-2656 (2014).
7. Y. Yuan, C. Chen, C. Zeng, B. Mousavi, S. Chaemchuen, F Verpoort, Carboxylation of Terminal Alkynes with Carbon Dioxide Catalyzed by an In Situ Ag_2O/N-Heterocyclic Carbene Precursor System. *Chem. Cat. Chem.* **9,** 882-887 (2017).
8. H. Cheng, B. Zhao, Y. Yao, C. Lu, Carboxylation of terminal alkynes with CO_2 catalyzed by bis(amidate) rare-earth metal amides. *Green Chem.* **17,** 1675-1682 (2015).